# Andersonian wrench faulting in a regional stress field during the 2010–2011 Canterbury, New Zealand, earthquake sequence

R. H. SIBSON[1]*, F. C. GHISETTI[2] & R. A. CROOKBAIN[3]

[1]*Department of Geology, University of Otago, P.O. Box 56, Dunedin 9054, New Zealand*

[2]*Terrageologica, 129 Takamatua Bay Rd., RD1, Akaroa 7581, New Zealand*

[3]*Shell Exploration NZ Ltd, 167 Devon Street West, New Plymouth 4310, New Zealand*

**Corresponding author (e-mail: rick.sibson@otago.ac.nz)*

**Abstract:** The initial $M_w$7.1 Darfield earthquake sequence was centred west of Christchurch City in the South Island of New Zealand but aftershocks, including a highly destructive $M_w$6.3 event, eventually extended eastwards across the city to the coast. The mainshock gave rise to right-lateral strike-slip of up to 5 m along the segmented rupture trace of a subvertical fault trending 085 $\pm$ 5° across the Canterbury Plains for *c*. 30 km, in agreement with teleseismic focal mechanisms. Near-field data however suggest that the mainshock was composite, initiating with reverse-slip north of the surface rupture. Stress determinations for the central South Island show maximum compressive stress $\sigma_1$ to be horizontal and oriented 115 $\pm$ 5°. The principal dextral rupture therefore lies at *c*. 30° to regional $\sigma_1$, the classic 'Andersonian' orientation for a low-displacement wrench fault. An aftershock lineament trending *c*. 145° possibly represents a conjugate left-lateral strike-slip structure. This stress field is also consistent with predominantly reverse-slip reactivation of NNE–NE faults along the Southern Alps range front. The main strike-slip fault appears to have a low cumulative displacement and may represent either a fairly newly formed fault in the regional stress field, or an existing subvertical fault that happens to be optimally oriented for frictional reactivation.

The $M_w$7.1 Darfield earthquake and ensuing aftershocks were initially largely restricted to the upper crust below the Canterbury Plains lying between Christchurch and the foothills of the Southern Alps in the South Island of New Zealand. The epicentral region lies about 100 km SE of the dextral-reverse Alpine Fault trending 050° and nearly the same distance SSE from the *c*. 070° trending dextral Hope Fault, which are principal fast-moving (20–30 mm $a^{-1}$) components of the Pacific–Australia plate boundary fault system (Fig. 1; note that all listed horizontal trends are given as 000–360° azimuthal bearings). The tectonic setting is one of continental convergence with local geology comprising a basement of Mesozoic greywackes (Rakaia Terrane) overlain unconformably by a Late Cretaceous–Tertiary cover sequence about 1 km in thickness, capped in turn by an upper Quaternary sequence of post-glacial alluvial gravels up to a few hundred metres thick (Forsyth *et al.* 2008). Following the earthquake, a subvertical strike-slip rupture with dextral displacements of up to 5 m was mapped east–west across the Canterbury Plains for *c*. 30 km (Quigley *et al.* 2010, 2012) (Fig. 2). The causative fault structures for the Darfield sequence had no prior topographic expression and were unrecognized before the event although parallel east–west trending faults, some clearly Holocene-active, had been recognized to the north, south and offshore to the east (e.g. Wood & Herzer 1993; Forsyth *et al.* 2008). In this note we explore the relationships between the principal strike-slip rupture and the tectonic stress field in the northern South Island.

## The 2010 Darfield earthquake sequence

The $M_w$7.1 mainshock of the 2010 Darfield earthquake sequence occurred at 04:35 local time on 4 September 2010 (16:35 UTC on September 3), initiating at a depth of 11 km below an extremely low-relief portion of the Canterbury Plains (Fig. 2). The epicentre was *c*. 6 km ESE from the town of Darfield some 38 km west of Christchurch city, and about 18 km SE of the foothills of the Southern Alps (Gledhill *et al.* 2011).

### *Surface rupture*

A segmented strike-slip rupture trace with right-lateral displacement averaging 2.5 m but ranging up to 5 m (now termed the Greendale Fault) was mapped east–west for *c*. 30 km across the Canterbury Plains (Quigley *et al.* 2010, 2012). The surface expression of the rupture in the alluvial gravels was that of a dextral Riedel shear array, typical of

*From*: HEALY, D., BUTLER, R. W. H., SHIPTON, Z. K. & SIBSON, R. H. (eds) 2012. *Faulting, Fracturing and Igneous Intrusion in the Earth's Crust*. Geological Society, London, Special Publications, **367**, 7–18. http://dx.doi.org/10.1144/SP367.2 

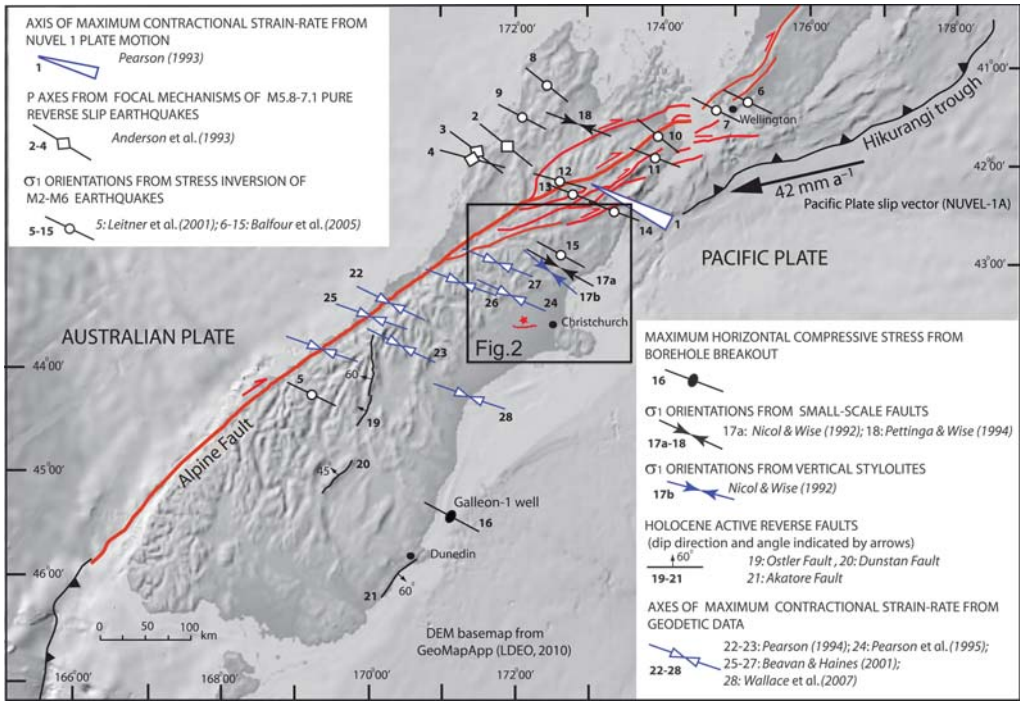


**Fig. 1.** Setting of the 2010–2011 Canterbury earthquake sequence west of Christchurch (red star denotes epicentre of the 4 September $M_w$7.1 Darfield mainshock; irregular bold red line is the surface rupture along the Greendale Fault) in relation to the main plate boundary fault system in the South Island of New Zealand. Insets list data sources for different stress indicators.

a buried right-lateral strike-slip fault propagating up through alluvial cover (cf. Tchalenko 1970). Measured displacements were consistent with pure dextral strike-slip on a subvertical fault with an enveloping surface for the left-stepping rupture segments striking 085°, on average. Notably, however, the surface rupture trace lies *c*. 8 km south of the well-constrained seismological epicentre (Gledhill *et al.* 2011).

## *Seismological characteristics*

Teleseismic moment tensor analyses from long-period waves (US Geological Survey; Harvard Global CMT Catalogs; http://earthquake.usgs.gov) yield focal mechanisms consistent with near-vertical dextral strike-slip on a rupture paralleling the mapped surface trace of the Greendale Fault. Near-field seismological and geodetic data however suggest that the mainshock was composite. Both first motion and regional moment tensor analyses yielded initial mechanisms involving reverse-slip on NE–SW striking planes lying north of the strike-slip surface trace (Gledhill *et al.* 2011). This initial reverse-slip is believed to have contributed to the high vertical accelerations (0.5–1.0 g) measured in the epicentral area.

## *Aftershocks*

Seven months after the $M_w$7.1 earthquake on 4 September 2010, nearly 5000 aftershocks had been recorded. These include one $M_w$6.3 event, 16 shocks in the range $5.9 > M_w > 5.0$ and 202 in the range $4.9 > M_w > 4.0$ (Fig. 2). A more complete structural analysis of the still ongoing sequence is given by Sibson *et al.* (2011). The great majority of the aftershocks were located at depths less than 15 km. Note that a strike-slip environment has the singular advantage that epicentre alignments can be used to map out subsidiary vertical faults if such occur (e.g. Fukuyama *et al.* 2003). Most of the aftershocks occur in an east–west swathe around the surface rupture trace of the Greendale Fault (Fig. 2), but a number of subsidiary clusters and lineaments are also evident (Gledhill *et al.* 2011). A cluster west of the western curving termination of the surface rupture abuts the foothills of the Southern Alps and is dominated by reverse-slip events. More diffuse activity occurs along the foothills to the NE.

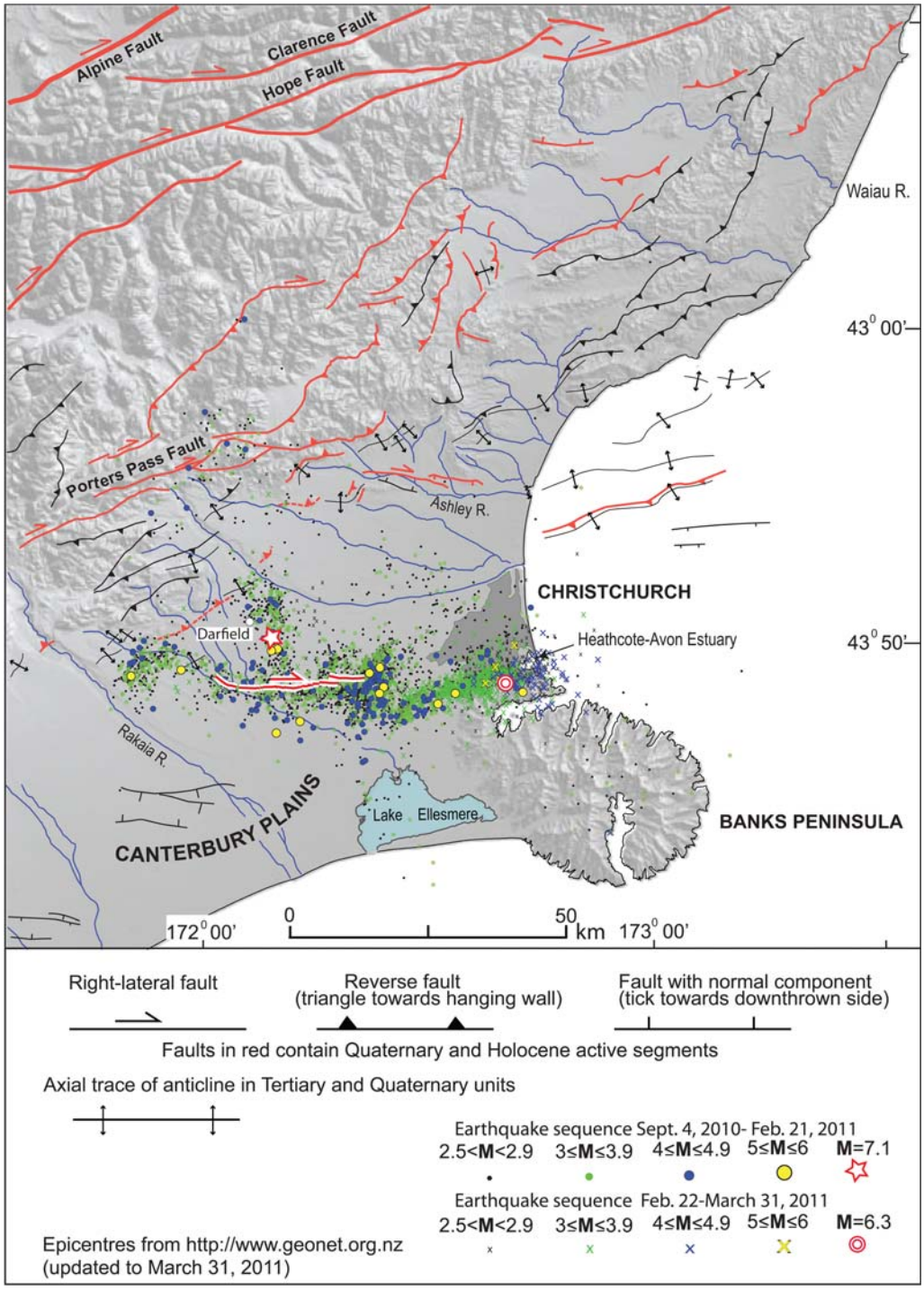


**Fig. 2.** Local setting of the 2010–2011 Darfield–Christchurch earthquake sequence in relation to mapped structures (after Rattenbury *et al.* 2006; Forsyth *et al.* 2008). Surface rupture accompanying the Darfield earthquake from Quigley *et al.* (2010) with distribution of mainshock and aftershock epicentres updated to 31 March 2011 from GEONET (http://www.geonet.org.nz). DEM from USGS/NASA Shuttle Radar Topography Mission v. 4 (http://srtm.csi.cgiar.org).

A subsidiary belt of activity trends NNW from the mainshock epicentre towards the foothills and the Porters Pass system of strike-slip faults. Of particular interest is a diffuse aftershock lineament developed south of the surface rupture in the first two weeks of the sequence, trending *c.* 145° towards the mouth of Lake Ellesmere (Fig. 2). A strong concentration of activity including five of the $M_w > 5.0$ events occurs at the eastern end of the surface rupture and just south of it, associated with a stepover (dilational?) to an ENE-trending en echelon aftershock lineament that continues eastwards (Fig. 2).

On 22 February (23:52 UTC on 21 February), central and eastern Christchurch were devastated by an $M_w$6.3 aftershock associated with the eastwards extension of this lineament. From focal mechanism and geodetic analyses, dextral-reverse oblique slip occurred over a rupture with dimensions 15 × 7 km oriented *c.* 060°/60°SE beneath the Heathcote–Avon estuary at depths from 1–7 km (Ristau *et al.* 2011). No surface fault break was observed but intensified aftershock activity continues, extending out to sea north of Banks Peninsula (Fig. 2).

## Regional stress in the South Island

A variety of seismological, geodetic and geological indicators suggest that regional maximum compressive stress $\sigma_1$ is horizontal and oriented WNE–ESE through much of the South Island (Fig. 1). The different indicators are listed on an azimuthal plot (Fig. 3) for comparison, with line solidity giving a qualitative indication of their reliability. Data are grouped for three domains: a Northern Domain covering approximately the top quarter of the South Island including the Marlborough faults; a Central Domain including north and south Canterbury (including Christchurch and the Darfield epicentral area) together with the central Southern Alps extending across the Alpine Fault into Westland; and a Southern Domain embracing Otago and Southland.

### *Stress inversions and focal mechanisms*

Stress inversions from crustal focal mechanisms led McGinty *et al.* (2000) to infer subhorizontal $\sigma_1$ stress trajectories oriented 120 and 118° in northern and southern Marlborough, respectively. Likewise, Balfour *et al.* (2005) carried out a comprehensive analysis of stress in the northern South Island and around the Marlborough fault system based on stress inversions from focal mechanisms, yielding a 'best-fit' horizontal $\sigma_1$ stress trajectory trending 115 ± 16° which is remarkably uniform across the northern South Island. These trajectories are consistent with *P*-axes determined for the 1968 $M_w$7.1 Inangahua earthquake and the 1991 $M_w$5.8 Hawks Crag I and $M_w$6.0 Hawks Crag II earthquakes in the northern South Island, all of which involved near-pure reverse-slip mechanisms (Anderson *et al.* 1993). In a study of seismicity around the Alpine Fault (mostly concentrated in its hanging wall below the Southern Alps) Leitner *et al.* (2001) carried out a series of stress inversions for various domains, finding a fairly constant subhorizontal $\sigma_1$ stress trajectory oriented 110–120°.

### *Galleon-1 borehole breakout*

Borehole breakouts, commonly assessed from dipmeter logs, are widely employed to determine the contemporary horizontal stress orientations (Zoback 2007). Generally, a vertical borehole coincides with one of the three principal compressive stresses. Initial elastic distortion of the approximately circular cross-section by the stress differential between the two horizontal principal compressive stresses ($\sigma_{H1} > \sigma_{H2}$) is amplified by induced shear fractures and spalling of the borehole walls because of stress concentrations at the areas of greatest curvature. This creates an oval cross-section to the borehole with the long axis at right angles to the maximum horizontal compressive stress, $\sigma_{H1}$. For an Andersonian strike-slip regime, the orientations of $\sigma_{H1}$ and $\sigma_{H2}$ correspond to $\sigma_1$ and $\sigma_3$, respectively, while for a thrust regime they correspond to $\sigma_1$ and $\sigma_2$, respectively.

The Galleon-1 well, drilled 25 km offshore from the south Canterbury coast in 1985 to a total depth of 3086 m (Wilson *et al.* 1985), provides the only breakout stress determination available to us. Systematically aligned breakouts were recorded in Late Cretaceous–Eocene strata from depths of 3018 to 2149 m. A high-resolution dipmeter tool (HDT) log was run in the 12.25″ diameter hole and a stratigraphic HDT log (SHDT) in the 8.5″ hole. Caliper and orientation data were available digitally for the HDT, while the pertinent SHDT data were digitized from a scan of the field print. For the purpose of this analysis the well is essentially vertical, deviating a maximum of 4° from the vertical along an azimuth of 246° at 2918 m. Azimuths derived from both logging tools were corrected for a magnetic declination of 23°E. Breakouts were analysed using the criteria proposed by Reinecker *et al.* (2003); the data are summarized in Table 1.

Note that the breakout azimuths vary slightly between the 12.25″ diameter and 8.5″ diameter sections of the borehole. Table 1 lists the mean breakout azimuth and standard deviation for the two hole diameters which are then aggregated over the entire logged interval. Cumulative breakout length totalled 268 m over six separate zones. The average breakout azimuth was 024 ± 9°, implying

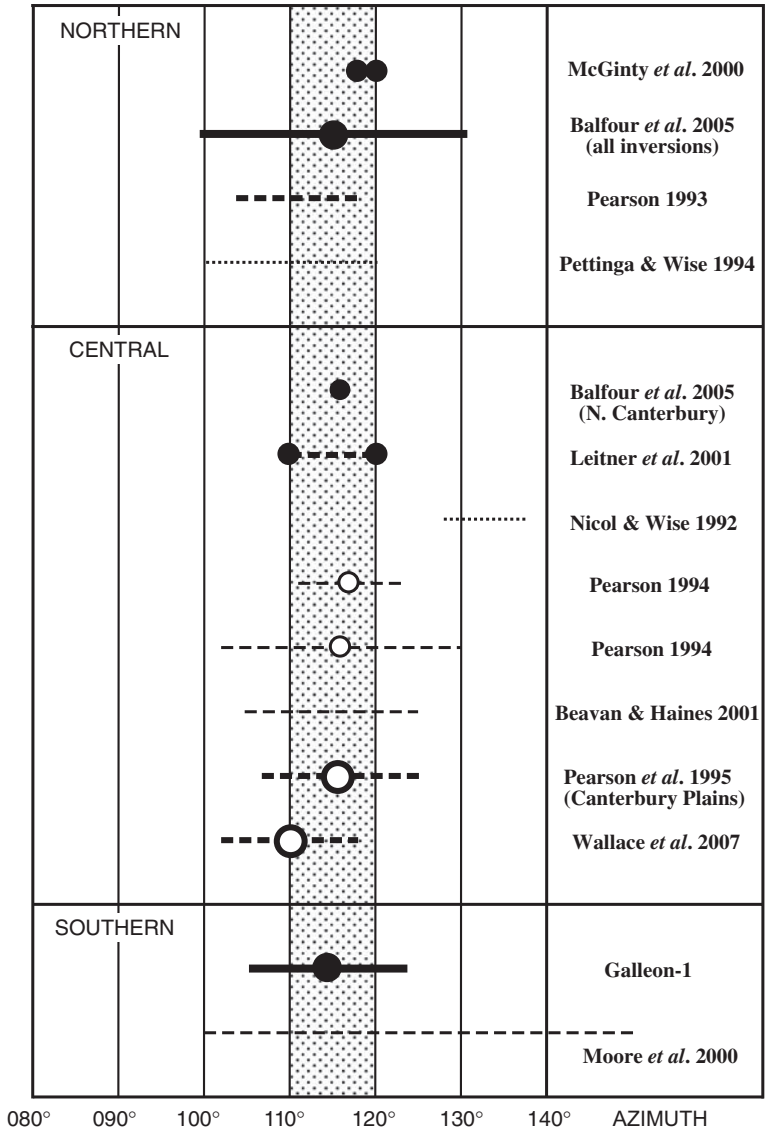


**Fig. 3.** Azimuthal plot for horizontal $\sigma_1$ stress indicators for the northern, central and southern South Island. Line thickness is a qualitative assessment of reliability. Solid circles, stress inversions from focal mechanisms or borehole breakouts (solid bars represent uncertainties where given); open circles, trends for maximum contractional strain rate (dashed bars represent uncertainties where given; dashed lines terminated by circles are range estimates); dotted lines, geological estimates of palaeostress orientation.

$\sigma_{H1}$ oriented $114 \pm 9^\circ$. Using criteria from the World Stress Map (Heidbach *et al.* 2010) this ranks as a B-quality determination on a 5-point scale.

### *Geodetic strain rate determinations*

Axes of maximum contractional strain rate have comparable trends to those inferred for $\sigma_1$ trajectories throughout much of the South Island (Figs 1 & 3). This parallelism is explicable if, over short time intervals without significant strain release from large earthquakes, maximum contractional strain rate is regarded as a measure of maximum incremental shortening subparallel to $\sigma_1$. Comparable relationships have been noted elsewhere (e.g. Keiding *et al.* 2009), but are not invariably the case

**Table 1.** *Frequency weighted breakout azimuths in the Galleon-1 well. Depths are recorded in metres measured along the hole below the rotary table (MAHBRT). Cumulative BO refers to the cumulative breakout length (m); R refers to the mean resultant length of the breakout sample unit vectors and is an indicator of angular dispersion (Fisher 1996)*

| Logged interval | Depth to top (m) | Depth to base (m) | Cumulative BO (m) | *R* | Mean BO azimuth | Standard deviation of BO azimuth |
|---|---|---|---|---|---|---|
| 12.25″ hole | 1930.1 | 2721.1 | 71 | 0.98 | 031.7° | 5.7° |
| 8.5″ hole | 2721.1 | 3078.0 | 197 | 0.97 | 019.1° | 7.1° |
| Total | 1930.1 | 3078.0 | 268 | 0.95 | 023.9° | 9.1° |

(Townend & Zoback 2006). Thus, Reilly (1990) inferred a regional compressive stress oriented at 110° from consideration of shear strain rates along the Hikurangi Margin. Similarly, Pearson (1993) extrapolated from the NUVEL-1 plate model (De Mets *et al*. 1990) to find a maximum contractional strain rate averaging 114–118° through the northern South Island. Wallace *et al.* (2007) employed a rotating elastic block model to describe active deformation in the South Island, determining a maximum contractional strain rate oriented 110 ± 8° within the Canterbury/Otago block which includes the area of the Darfield earthquake sequence.

In more local studies, Pearson (1994) found comparably oriented axes of maximum contractional strain rate from areas west and east of the Alpine Fault in the central South Island: 117 ± 6° for the Okarito network and 116 ± 14° for the Godley Valley region. In the area of the Canterbury Plains NW of Christchurch, Pearson *et al.* (1995) found the maximum contractional strain rate to be oriented 116 ± 9° just north of the Darfield epicentral area. From inversion of modern GPS networks in the central Southern Alps further west, Beavan & Haines (2001) determined maximum contractional strain rates trending from 105 to 115°. Strain rates are significantly lower in the southern South Island (Otago and Southland) and are less well constrained. From repeated triangulation surveys, Walcott (1984) found maximum contractional strain rates in Southland oriented 103 ± 18° while Moore *et al.* (2000) found an azimuthal range of 100–150°. Given these uncertainties, the Galleon-1 borehole determination seems likely to be the most reliable indicator of regional stress in the southern South Island.

## *Geological indicators of regional stress*

Comparatively few palaeostress determinations have been carried out from neotectonic studies in the South Island and the age of the deformation is often not well constrained. Nicol & Wise (1992) infer a subhorizontal $\sigma_1$ palaeostress trending 133 ± 5° from a systematic set of subvertical stylolitic solution surfaces in Oligocene limestone plus related minor structures in the Doctor's Dome area of north Canterbury, which they infer to be probably of Late Pliocene–Early Pleistocene age. From slickenline analysis of minor faults of probable Miocene–Pliocene age around the Waimea Fault near Nelson, Pettinga & Wise (1994) deduced an overall subhorizontal $\sigma_1$ palaeostress trending 110–120°. Because of the age uncertainty, these palaeostress indicators are ranked low in terms of reliability.

Crude constraints on present stress-field orientation come from the lack of obvious strike-slip on several major reverse faults that are Holocene-active, restricting the $\sigma_1$ stress trajectory to lie nearly orthogonal to strike (Fig. 1). The Ostler Fault strikes 010–030° through the McKenzie Basin south of Mount Cook (Ghisetti *et al.* 2007), implying a $\sigma_1$ trajectory oriented 100–120°. Likewise, Quaternary active traces of the Dunstan Fault in Central Otago, which Beanland *et al.* (1986) regard as a pure reverse-slip structure, strike 033° on average, implying $\sigma_1$ trending 123°. Further south, the Akatore Fault strikes 035–040° (Litchfield & Norris 2000) implying $\sigma_1$ oriented 125–130°. The uncertainties, however, are considerable. For a fault with dip $\delta$ and a horizontal slip vector oblique to the fault dip direction by an angle $\phi$, the ratio of horizontal to vertical displacement is $H/V = \tan\delta \tan\phi$. On the grounds that a strike-slip component will only become geomorphically obvious when the horizontal displacement exceeds the vertical displacement (i.e. $H/V > 1$), this allows the obliquity of the slip vector to range $\pm 45°$ from the strike-normal direction for $\delta = 45°$. Because of the large uncertainties, these estimates of possible $\sigma_1$ trends are therefore omitted from Figures 1 and 3. Principal Horizontal Shortening (PHS) directions obtained by Berryman (1979) from H/V analysis of active faults throughout the South Island are not greatly dissimilar from the $\sigma_1$ trajectories illustrated in Figures 1 and 3, however.

## *Estimated stress field for the Darfield–Christchurch earthquake sequence*

While recognizing that local stress heterogeneity may occur, a remarkably consistent picture of the

regional stress field emerges from Figures 1 and 3 for the northern and central South Island especially if one accepts axes of maximum contractional strain rate as proxies for $\sigma_1$ trajectories. We therefore adopt a $\sigma_1$ trajectory trending $115 \pm 5^\circ$ as the best estimate for the regional stress field in the area of the Darfield earthquake sequence. This is in fact nearly identical to the $\sigma_1$ trajectory derived for north Canterbury by Balfour *et al.* (2005) in the southernmost of their stress inversions from focal mechanisms (Fig. 3). It is also comparable with the stress orientations for the northern South Island listed in the 2008 World Stress Map that are derived entirely from focal mechanism inversions (Heidbach *et al.* 2010). Note that this $\sigma_1$ orientation is also consistent with predominantly reverse-slip reactivation of structures trending NNE–NE along the Southern Alps range front. Given the mixture of strike-slip and reverse faulting in the Darfield sequence, it seems likely that the stress field is of the form $\sigma_1 > \sigma_v = \sigma_2 \sim \sigma_3$ with local variance between $\sigma_v = \sigma_2$ and $\sigma_v = \sigma_3$.

## Stress controls on the initiation and reactivation of strike-slip faults

### *Initiation of Andersonian wrench (strike-slip) faults*

Anderson (1905, 1951) recognized three fundamental stress regimes within the crust, depending which of the principal compressive stresses ($\sigma_1 > \sigma_2 > \sigma_3$) lies vertical in accordance with the boundary condition imposed by the Earth's free surface. He then argued that this should give rise to three basic classes of fault (normal faults when $\sigma_v = \sigma_1$; wrench faults when $\sigma_v = \sigma_2$; thrust faults when $\sigma_v = \sigma_3$) forming in accordance with the Coulomb criterion for brittle shear failure which, for a fluid-saturated rock mass with pore-fluid pressure $P_f$ may be written:

$$\tau = C + \mu_i \sigma_n' = C + \mu_i(\sigma_n - P_f) \qquad (1)$$

where $\tau$ and $\sigma_n$ are the shear and normal stress components on the failure plane, respectively, and the intact rock is characterized by a cohesive strength $C$ and a coefficient of internal friction $\mu_i = \tan \phi_i$ (the friction angle $\phi_i$ being the slope of the failure envelope on a Mohr diagram; Jaeger & Cook 1979). Shear failure then occurs on planes containing the $\sigma_2$ direction oriented at an angle to the maximum compression $\sigma_1$ given by:

$$\theta_i = 45^\circ - \frac{\phi_i}{2} = 0.5 \tan^{-1}\left(\frac{1}{\mu_i}\right). \qquad (2)$$

From experimental rock mechanics, internal friction generally lies in the range $0.5 < \mu_i < 1.0$ (Jaeger & Cook 1979) so that new faults should lie at $32^\circ > \theta_i > 22^\circ$ to $\sigma_1$ and contain the $\sigma_2$ axis. For the particular case where $\sigma_v = \sigma_2$, wrench (strike-slip) faults should develop along vertical planes lying at $22–32^\circ$ to horizontal $\sigma_1$, with the possibility of conjugate wrench faults forming at a dihedral angle of $44–64^\circ$ (Fig. 4). While rock anisotropy may cause significant deviations from these idealized relationships, they often appear to hold for brittle strike-slip faults with low cumulative displacement (e.g. Anderson 1951; Kelly *et al.* 1998).

### *Frictional reactivation of strike-slip faults*

Reshear of an existing fault retaining some cohesive strength $c$ (generally $c < C$, but may be vanishingly small at low normal stresses; Byerlee 1978) is of similar form:

$$\tau = c + \mu_s \sigma_n' = \mu_s(\sigma_n - P_f) \qquad (3)$$

where $\tau$ and $\sigma_n$ are again the shear and normal stress components on the fault plane, $P_f$ is the pore-fluid pressure and $\mu_s$ is the coefficient of frictional sliding on the existing plane. Consider the case of an existing fault containing the $\sigma_2$ axis oriented at a reactivation angle $\theta_r$ to $\sigma_1$ (Fig. 4). The optimal orientation of the fault with respect to $\sigma_1$ for frictional reactivation (when the differential stress required for reshear is a minimum) is given by:

$$\theta_r^* = 0.5 \tan^{-1}\left(\frac{1}{\mu_s}\right). \qquad (4)$$

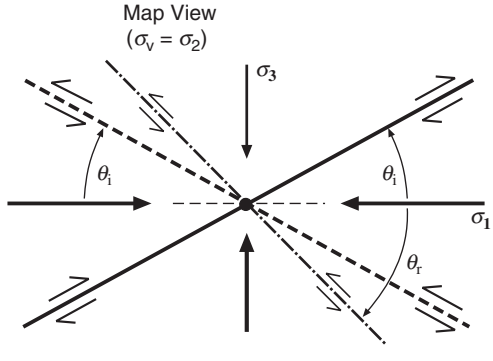


**Fig. 4.** Cartoon map illustrating a regional 'wrench fault' stress regime with $\sigma_v = \sigma_2$ and the expected orientations of a new-forming Andersonian dextral strike-slip fault and conjugate sinistral fault at $\pm\theta_i$ to $\sigma_1$. Also shown is the reactivation angle $\theta_r$ defined with respect to $\sigma_1$ for an existing vertical fault containing the $\sigma_2$ axis (dash-dot line).

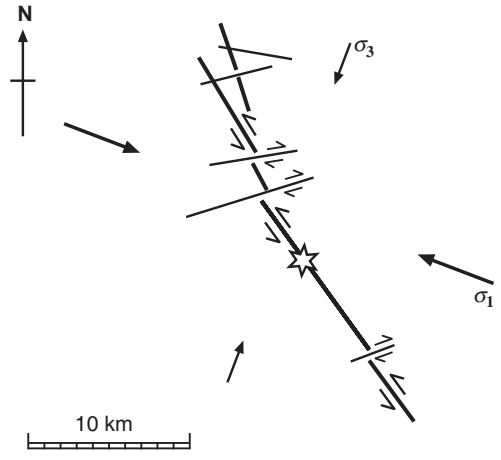


**Fig. 5.** 2000 $M_w$6.6 Western Tottori earthquake and inferred stress field (after Ohmi *et al.* 2002; Fukuyama *et al.* 2003). Star, instrumental epicentre; bold lines, main left-lateral strike-slip rupture defined by aftershocks; thinner lines, conjugate right-lateral faults defined by aftershock lineaments.

Note that $\theta_r^*$ is always $\leq 45^\circ$. In an extensive set of experiments, Byerlee (1978) demonstrated that for most rocks $0.6 < \mu_s < 0.85$ so that (generally) $30^\circ > \theta_r^* > 25^\circ$. In fact, $\theta_r^*$ remains within $30 \pm 5^\circ$ over the broad range of friction coefficients of $0.36 < \mu_s < 0.84$. Faults therefore reactivate most easily when oriented close to their original Andersonian attitudes. While reactivation may occur at $\theta_r < \theta_r^*$ and $\theta_r > \theta_r^*$, frictional lock-up occurs at $\theta_r = 2\theta_r^*$, prohibiting reshear at higher reactivation angles unless the tensile overpressure condition $P_f > \sigma_3$ is met (Sibson 1985).

### *2000 $M_w$6.6 Western Tottori earthquake: Andersonian wrench faulting in action*

The previously unrecognized fault that ruptured in the 2000 $M_w$6.6 Western Tottori earthquake in SW Honshu, Japan, is an example of an active strike-slip fault (probably of low cumulative displacement) that approximates to Andersonian character (Fig. 5). No definite surface rupturing was recognized, but focal mechanism analysis and a well-defined planar distribution of aftershocks showed that left-lateral strike-slip rupturing with maximum slip ranging up to *c.* 5 m occurred for over 30 km along strike and to a depth of about 12 km, on a subvertical fault striking 145–150° on average (Ohmi *et al.* 2002; Fukuyama *et al.* 2003; Yukutake *et al.* 2007). The high-resolution aftershock study also shows that the principal NNW–SSE fault is cross-cut and dextrally offset along a set of subsidiary aftershock lineaments defining conjugate right-lateral strike-slip faults at dihedral angles ranging between 45 and 75° (Fig. 6). Although some of these dihedral angles are somewhat in excess of those anticipated from experimental rock

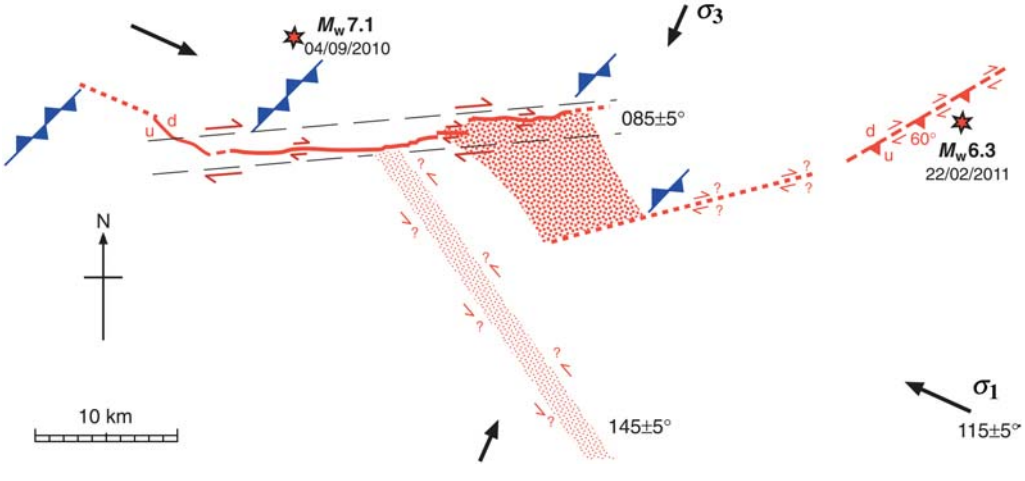


**Fig. 6.** Seismotectonic cartoon for the 2010–2011 Darfield–Christchurch earthquake sequence. Stars, instrumental epicentres for major shocks; bold red lines, dextral strike-slip surface rupture along Greendale Fault accompanying the 4 September $M_w$7.1 earthquake (after Quigley *et al.* 2010); dotted red lines, inferred subsurface extensions of surface rupture and aftershock lineaments; dashed toothed red line, inferred dextral-reverse rupture for 22 February $M_w$6.3 earthquake (Ristau *et al.* 2011); double-toothed blue lines, inferred strike traces of subsurface reverse-slip ruptures (dips uncertain); light stippled band, Norwood–Doyleston–Ellesmere aftershock lineament with inferred left-lateral strike-slip; heavy stippled area, concentrated aftershock activity within possible dilational stepover.

deformation (44–64°), this could result from finite deformation and/or the presence of inherited structures favourably oriented for reactivation. Some stress field heterogeneity is evident locally, but stress inversions from aftershock focal mechanisms define an Andersonian wrench regime with $\sigma_2$ subvertical and subhorizontal $\sigma_1$ trending $115 \pm 10^\circ$ (Fukuyama *et al.* 2003; Yukutake *et al.* 2007). The vertical left-lateral strike-slip fault therefore lies at $30 \pm 10^\circ$ to regional $\sigma_1$ trajectories. Together, the vertical fault plane containing $\sigma_2$, the reactivation angle of *c.* 30° and the set of conjugate dextral faults are all consistent with wrench fault development as envisaged by Anderson (1905).

### *Stress and large-displacement strike-slip faults*

Simple Andersonian relationships between regional $\sigma_1$ trajectories and fault orientation do not seem to hold for large-displacement continental strike-slip faults. Although some stress heterogeneity is apparent, horizontal $\sigma_1$ trajectories lie at up to 85° to the trace of the San Andreas fault in central California and at 60–70° to the fault in southern California (Mount & Suppe 1987; Zoback *et al.* 1987; Townend & Zoback 2004). Likewise, stress inversions in the northern South Island suggest horizontal $\sigma_1$ trajectories lying at *c.* 60° to the main strands of the Marlborough fault system (Balfour *et al.* 2005). These relationships may be explained, at least in part, by the significant block rotations expected to occur about vertical axes in areas of distributed continental deformation (Nur *et al.* 1986; Lamb 1988). Nonetheless, continued slip activity on these structures, oriented at beyond frictional lock-up for Byerlee's (1978) friction values, implies extreme weakness of the large-displacement faults that is not easily accounted for either by the presence of low-friction fault material or by near-lithostatic fluid overpressures.

## Regional stress and the 2010 Darfield earthquake sequence

A seismotectonic cartoon (Fig. 6) illustrates the geometrical relationships between the regional stress field (horizontal $\sigma_1$ trending $115 \pm 5^\circ$) and the principal subvertical strike-slip rupture striking $085 \pm 5^\circ$ in the Darfield sequence (Greendale Fault), along with other subsidiary features defined by the aftershock distribution and focal mechanisms provided by Gledhill *et al.* (2011). The subvertical dextral strike-slip rupture lies at $30 \pm 10^\circ$ to inferred $\sigma_1$, the expected relationship for a new-formed strike-slip fault (Anderson 1905) or for an existing fault at the optimal orientation for frictional reactivation in a stress field with $\sigma_v = \sigma_2$.

Note that the western termination of the Greendale Fault surface rupture, which exhibits a component of normal slip (Quigley *et al.* 2010), curves NW to lie subperpendicular to the inferred $\sigma_3$ direction. At the eastern termination of the Greendale surface rupture, a rhomboidal area of concentrated aftershock activity with mixed strike-slip and extensional normal faulting (Gledhill *et al.* 2011) defines a stepover structure to an en echelon microearthquake lineament trending ENE towards the Heathcote–Avon estuary. This is the typical expression of a dilational stepover in a dextral strike-slip fault system (Sibson 1986); such features are commonly associated with time-dependent slip transfer to the en echelon fault segment. During the 22 February $M_w$6.3 aftershock, dextral-reverse oblique slip occurred on a more northerly striking (*c.* 060°) fault dipping *c.* 60°SE from below the Heathcote–Avon estuary (Ristau *et al.* 2011). While this major aftershock likely involves reactivation of an inherited fault structure, the kinematics remain compatible with the inferred stress field (Fig. 6).

Within such a regional stress regime, a conjugate left-lateral strike-slip fault would be expected to be subvertical and strike *c.* $145 \pm 5^\circ$, which is the approximate trend of an aftershock lineament (Norwood–Doyleston–Ellesmere lineament) discernible south of the Greendale rupture running SE towards the mouth of Lake Ellesmere (Figs 2 & 6). Left-lateral strike-slip along a lineament of this orientation is compatible with a number of the focal mechanisms provided for this area by Gledhill *et al.* (2011). If this 145° trending lineament is indeed a left-lateral strike-slip fault, it confirms the inferred 115° trend for the regional $\sigma_1$ trajectory in the area of the Darfield earthquake sequence. A degree of aftershock clustering occurs around the intersection of the two lineaments. It seems likely that sinistral strike-slip along this subsidiary lineament may be interfering with the main dextral fault structure, offsetting it left-laterally to create a local contractional jog as occurs further east along the segmented rupture trace. A mesh structure of conjugate right- and left-lateral faults may contribute to areas of distributed aftershock activity.

Predominantly reverse-slip rupturing on NNE–NE striking planes in the area of the mainshock epicentre south of Darfield and immediately SW of the western termination of the Greendale rupture is also broadly compatible with the inferred $\sigma_1$ trajectory, but with $\sigma_v = \sigma_3$. Given the preponderant mixture of strike-slip and reverse fault aftershocks in the Darfield sequence, it seems likely that the stress field is transitional between a wrench and a thrust regime with $\sigma_1 > \sigma_v = \sigma_2 \sim \sigma_3$.

## Conclusions

Not withstanding the evidence of reverse-slip associated with the nucleation of the mainshock rupture (Gledhill *et al.* 2011), right-lateral strike-slip rupturing along a subvertical plane oriented at $30 \pm 10^{\circ}$ to regional $\sigma_1$ trajectories trending $115 \pm 5^{\circ}$ together with possible conjugate left-lateral faults at *c*. $60^{\circ}$ to the principal rupture (Fig. 6) all indicate a classic Andersonian wrench regime with $\sigma_v = \sigma_2$ (Anderson 1905, 1951). The structural geometry is comparable to the evidence for conjugate Andersonian wrench faulting visible in the aftershock distribution of the 2000 $M_w$6.6 Western Tottori earthquake in central Honshu, Japan, where the main left-lateral strike-slip fault structure is offset by a set of conjugate right-lateral strike-slip faults oriented at $50–70^{\circ}$ to the main structure (Ohmi *et al.* 2002; Fukuyama *et al.* 2003).

Orientation of the main dextral structure (the Greendale Fault) at the optimal angle for reactivation coupled with the evidence of persistent activity on conjugate structures makes it likely that the cumulative strike-slip on the Greendale Fault is comparatively low (<1 km?). It could represent either a fault that is fairly new-formed in the contemporary stress field or an existing subvertical fault that is optimally oriented for reshear in the stress field. From the complexity of the subsidiary aftershock trends and their disparate mechanisms it appears probable that the structure is growing by amalgamating inherited basement structures, perhaps largely derived from Late Cretaceous–Paleogene extensional tectonics (Field *et al.* 1989), with optimally oriented strike-slip segments formed in the contemporary stress field. With time and increasing displacement, the east–west Greendale Fault will likely evolve into a 'smoother' less complex strike-slip fault (Wesnousky 1988) and will perhaps rotate progressively towards parallelism with the ENE-trending faults to the north and become integrated into the Marlborough fault system.

We express our thanks to OMV New Zealand LTD and their joint venture partners Mitsui E&P Australia Pty Ltd and PTTEP New Zealand LTD for permission to publish the results of the Galleon-1 breakout analysis and to Occam Technology PTY for digitization of HDT and SHDT field data. Thanks also to M. Reyners, J. Beavan and J. Townend for helpful discussions on the aftershock distribution and focal mechanisms and on stress/strain rate relationships. Helpful comments from M. Tingay and an anonymous reviewer significantly improved the manuscript.

## References

Anderson, E. M. 1905. The dynamics of faulting. *Transactions of the Edinburgh Geological Society*, **8**, 387–402.

Anderson, E. M. 1951. *The Dynamics of Faulting and Dyke Formation with Application to Britain*. 2nd edn. Oliver & Boyd, Edinburgh.

Anderson, H., Webb, T. & Jackson, J. 1993. Focal mechanisms of large earthquakes in the South Island of New Zealand: implications for the accommodation of Pacific-Australia plate motion. *Geophysical Journal International*, **115**, 1032–1054.

Balfour, N. J., Savage, M. K. & Townend, J. 2005. Stress and crustal anisotropy in Marlborough, New Zealand: evidence for low fault strength and structure-controlled anisotropy. *Geophysical Journal International*, **163**, 1073–1086.

Beanland, S., Berryman, K. R., Hull, A. G. & Wood, P. R. 1986. Late Quaternary deformation at the Dunstan Fault, Central Otago, New Zealand. *Royal Society of New Zealand Bulletin*, **24**, 293–306.

Beavan, J. & Haines, J. 2001. Contemporary horizontal velocity and strain-rate fields of the Pacific-Australia plate boundary zone through New Zealand. *Journal of Geophysical Research*, **106**, 741–770.

Berryman, K. 1979. Active faulting and derived PHS directions in the South island, New Zealand. *Royal Society of New Zealand Bulletin*, **18**, 29–34.

Byerlee, J. D. 1978. Friction of rocks. *Pure & Applied Geophysics*, **116**, 615–626.

De Mets, C., Gordon, R. G., Argus, D. F. & Stein, S. 1990. Current plate motions. *Geophysical Journal International*, **101**, 425–478.

Field, B. D., Browne, G. H. *et al.* 1989. *Cretaceous and Cenozoic Sedimentary Basins and Geological Evolution of the Canterbury Region, South Island, New Zealand. New Zealand Geological Survey Basin Studies 2*. Department of Scientific and Industrial Research, Wellington.

Fisher, N. I. 1996. *Statistical Analysis of Circular Data*. Cambridge University Press, UK.

Forsyth, P. J., Barrell, D. J. A. & Jongens, R. 2008. *Geology of the Christchurch area. Geological Map 16, 1:250,000*. GNS Science, Lower Hutt, New Zealand.

Fukuyama, E., Ellsworth, W. L., Waldhauser, F. & Kubo, A. 2003. Detailed fault structure of the 2000 Western Tottori, Japan, earthquake sequence. *Bulletin of the Seismological Society of America*, **93**, 1468–1478.

Ghisetti, F. C., Gorman, A. R. & Sibson, R. H. 2007. Surface breakthrough of a basement fault by repeated seismic slip episodes: the Ostler Fault, South Island, New Zealand. *Tectonics*, **26**, TC6004, doi: 10.1029/2007TC002146.

Gledhill, K., Ristau, J., Reyners, M., Fry, B. & Holden, C. 2011. The Darfield (Canterbury, New Zealand) $M_w$ 7.1 earthquake of September 4 2010: a preliminary seismological report. *Seismological Research Letters*, **82**, 378–386.

Heidbach, O., Tingay, M., Barth, A., Reinecker, J., Kurfeβ, D. & Müller, B. 2010. Global crustal stress pattern based on the World Stress Map database release 2008. *Tectonophysics*, **482**, 3–15.

Jaeger, J. C. & Cook, N. G. W. 1979. *Fundamentals of Rock Mechanics*. 3rd edn. Chapman & Hall, London.

Keiding, M., Lund, B. & Árnadóttir, T. 2009. Earthquakes, stress, and strain along an obliquely divergent

plate boundary: Reykjanes Peninsula, southwest Iceland. *Journal of Geophysical Research*, **114**, B09306, doi: 10.1029/2008JB006253.

KELLY, P. G., SANDERSON, D. J. & PEACOCK, D. C. 1998. Linkage and evolution of conjugate strike-slip fault zones in limestones of Somerset and Northumbria. *Journal of Structural Geology*, **20**, 1477–1493.

LAMB, S. H. 1988. Tectonic rotations about vertical axes during the last 4 Ma in part of the New Zealand plate-boundary zone. *Journal of Structural Geology*, **10**, 875–893.

LEITNER, B., EBERHART-PHILLIPS, D., ANDERSON, H. & NABELEK, J. 2001. A focused look at the Alpine Fault, New Zealand: seismicity, focal mechanisms and stress observations. *Journal of Geophysical Research*, **106**, 2193–2220.

LITCHFIELD, N. J. & NORRIS, R. J. 2000. Holocene motion on the Akatore fault, south Otago coast, New Zealand. *New Zealand Journal of Geology and Geophysics*, **43**, 405–418.

MCGINTY, P., REYNERS, M. & ROBINSON, R. 2000. Stress directions in the shallow part of the Hikurangi subduction zone, New Zealand, from the inversion of earthquake first motions. *Geophysical Journal International*, **142**, 339–350.

MOORE, M. A., ANDERSON, H. J. & PEARSON, C. 2000. Seismic and geodetic constraints on plate boundary deformation across the northern Macquarie Ridge and southern South Island of New Zealand. *Geophysical Journal International*, **143**, 847–880.

MOUNT, V. S. & SUPPE, J. 1987. State of stress near the San Andreas fault. *Geology*, **15**, 1143–1146.

NICOL, A. & WISE, D. U. 1992. Paleostress adjacent to the Alpine Fault of New Zealand: fault, vein, and stylolite data from the Doctors Dome area. *Journal of Geophysical Research*, **97**, 17 685–17 692.

NUR, A., RON, H. & SCOTTI, O. 1986. Fault mechanics and the kinematics of block rotations. *Geology*, **14**, 746–749.

OHMI, S., WATANABE, K., SHIBUTANI, T., HIRANO, N. & NAKAO, S. 2002. The 2000 Western Tottori earthquake – seismic activity revealed by the regional seismic networks. *Earth Planets Space*, **54**, 819–830.

PEARSON, C. 1993. Rate of coseismic strain release in the northern South Island, New Zealand. *New Zealand Journal of Geology and Geophysics*, **36**, 161–166.

PEARSON, C. 1994. Geodetic strain determinations from the Okarito and Godley-Tekapo regions, central South Island, New Zealand. *New Zealand Journal of Geology and Geophysics*, **37**, 309–318.

PEARSON, C., BEAVAN, J., DARBY, D., BLICK, G. H. & WALCOTT, R. I. 1995. Strain distribution across the Australian-Pacific plate boundary in the central South Island, New Zealand, from 1992 GPS and earlier terrestrial observations. *Journal of Geophysical Research*, **100**, 22 071–22 081.

PETTINGA, J. R. & WISE, D. U. 1994. Paleostress adjacent to the Alpine fault: broader implications from fault analysis near Nelson, South Island, New Zealand. *Journal of Geophysical Research*, **99**, 2727–2736.

QUIGLEY, M., VILLAMOR, P. *ET AL.* 2010. Previously unknown fault shakes New Zealand's South Island. *EOS, Transactions American Geophysical Union*, **91**, 469–472.

QUIGLEY, M., VAN DISSEN, R. *ET AL.* 2012. Surface rupture during the 2010 $M_w$ 7.1 Darfield (Canterbury) earthquake: implications for fault rupture dynamics and seismic-hazard analysis. *Geology*, **40**, 55–58.

RATTENBURY, M. S., TOWNSEND, D. B. & JOHNSTON, M. R. 2006. *Geology of the Kaikoura Area. Geological Map 13, 1:250,000.* GNS Science, Lower Hutt, New Zealand.

REILLY, W. I. 1990. Horizontal crustal deformation on the Hikurangi Margin. *New Zealand Journal of Geology and Geophysics*, **33**, 393–400.

REINECKER, J., TINGAY, M. & MÜLLER, B. 2003. *Borehole breakout analysis from four-arm caliper logs*. World Stress Map Project Stress Analysis Guidelines (available online at www.world-stress-map.org).

RISTAU, J., BANNISTER, S. *ET AL.* 2011. The $M_w$6.3 Christchurch, New Zealand, earthquake of 22 February 2011: preliminary seismic and geodetic results (Abstract). *Seismological Society of America 2011 Annual Meeting*, April 13–15, Memphis Tennessee.

SIBSON, R. H. 1985. A note on fault reactivation. *Journal of Structural Geology*, **7**, 751–754.

SIBSON, R. H. 1986. Rupture interaction with fault jogs. *In:* DAS, S., BOATWRIGHT, J. & SCHOLZ, C. H. (eds) *Earthquake Source Mechanics*. American Geophysical Union, Washington, Monograph 37 (Maurice Ewing Series 6), 157–167.

SIBSON, R. H., GHISETTI, F. C. & RISTAU, J. 2011. Stress control of an evolving strike-slip fault system during the 2010-2011 Canterbury, New Zealand, earthquake sequence. *Seismological Research Letters*, **82**, 824–832.

TCHALENKO, J. S. 1970. Similarities between shear zones of different magnitudes. *Geological Society of America Bulletin*, **81**, 1625–1640.

TOWNEND, J. & ZOBACK, M. D. 2004. Regional tectonic stress near the San Andreas fault in central and southern California. *Geophysical Research Letters*, **31**, L15S11, doi: 10.1029/2003GL018918.

TOWNEND, J. & ZOBACK, M. D. 2006. Stress, strain, and mountain building in central Japan. *Journal of Geophysical Research*, **111**, B03411, doi: 10.1029/2005JB003759.

WALCOTT, R. I. 1984. The kinematics of the plate boundary zone through New Zealand: a comparison of short-and long-term deformations. *Geophysical Journal of the Royal Astronomical Society*, **79**, 613–633.

WALLACE, L. M., BEAVAN, J., MCCAFFREY, R., BERRYMAN, K. & DENYS, P. 2007. Balancing the plate motion budget in the South Island, New Zealand, using GPS, geological and seismological data. *Geophysical Journal International*, **168**, 332–352.

WESNOUSKY, S. G. 1988. Seismological and structural evolution of strike-slip faults. *Nature*, **335**, 340–343.

WILSON, I. R., RENTON, P. H., MOUND, D. G. & GRANT, J. 1985. *Galleon-1 Geological Completion Report PPL 38203*, BP Shell Todd (Canterbury) Services. Unpublished Petroleum Report PR 1146 (http://www.crownminerals.govt.nz).

WOOD, R. A. & HERZER, R. H. 1993. The Chatham Rise, New Zealand. *In:* BALLANCE, P. F. (ed.) *South Pacific Sedimentary Basins*, *Sedimentary Basins of the World 2*. Elsevier, Amsterdam, 329–349.

YUKUTAKE, Y., IIO, Y., KATAO, H. & SHIBUTANI, T. 2007. Estimate of the stress field in the region of the 2000 Western Tottori earthquake: using numerous aftershock focal mechanisms. *Journal of Geophysical Research*, **112**, B09306, doi: 10.1029/2005JB004250.

ZOBACK, M. D. 2007. *Reservoir Geomechanics*. Cambridge University Press, Cambridge.

ZOBACK, M. D., ZOBACK, M. L. *ET AL.* 1987. New evidence on the state of stress on the San Andreas fault system. *Science*, **238**, 1105–1111.